Crystal and electronic structure of superhard BC_5: First-principles structural optimizations

Yansun Yao,[1] John S. Tse,[2,*] and Dennis D. Klug[1]
[1]*Steacie Institute for Molecular Sciences, National Research Council of Canada, Ottawa, Ontario, Canada K1A 0R6*
[2]*Department of Physics and Engineering Physics, University of Saskatchewan, Saskatoon, Saskatchewan, Canada S7N 5E2*
(Received 23 April 2009; revised manuscript received 18 August 2009; published 16 September 2009)

A thermodynamically stable $I\bar{4}m2$ phase of superhard BC_5 was predicted from exhaustive structural searches combined with first-principles structural optimizations. From the computed bulk and shear moduli, this phase is expected to be harder than the recently synthesized BC_5 with the diamond structure. The stability and strength are attributed to multicenter B-C-B interactions when two B atoms are linked through a common C atom. The $I\bar{4}m2$ phase is metallic and superconducting with an estimated superconducting critical temperature (T_c) of 47 K. Another candidate structure with $P\bar{1}$ symmetry was obtained and this fits well to the reported x-ray diffraction pattern. B atoms in the $P\bar{1}$ structure are not linked together by C atoms which yields higher energy. $P\bar{1}$ and $I\bar{4}m2$ structures have almost identical predicted hardness.

DOI: 10.1103/PhysRevB.80.094106 PACS number(s): 71.15.Mb, 74.10.+v, 74.25.Jb

Diamond is one of the most important materials due to its extreme hardness, optical transparency, and high room-temperature thermal conductivity.[1] The demand for superhard materials in industrial usages has stimulated research in the synthesis of alternate hard materials. Boron carbide (B_4C) is one of the hardest materials and ranks third behind diamond and cubic boron nitride.[2] Recently, using high-temperature high pressure (HPHT), a BC_5 phase was synthesized and quench recovered.[3] Compared to diamond with a Vicker's hardness 115 GPa, the measured hardness of BC_5 (71 GPa) exceeds that of *c*-BN (62 GPa).[3] This BC_5 phase[3] has a similar x-ray diffraction pattern as diamond. However, details of its crystal structure are not yet known. B has a strong tendency to segregate in electron-deficient B-C systems and the presence of icosahedral B_{12} units are ubiquitous.[4] To characterize the structure and electronic properties of the superhard BC_5, structural searches, electronic-structure and vibrational calculations with first-principles methods were performed. The present results suggest that the BC_5 structure observed in experiment has a x-ray diffraction pattern consistent with that of a homogeneously B-doped diamond structure with $P\bar{1}$ symmetry. The most stable structures, however, prefer two-dimensional (2D) clustering of B atoms. The multicenter bonding between two nearest-neighbor B atoms and the C atom connecting them increases the structural stability. It is predicted that the BC_5 polymorphs with 2D B clustering and homogeneous B doping should have similar hardness values. Furthermore, 2D B clustering also favors strong electron-phonon coupling (EPC) suggesting that these polymorphs may be superconducting.

Two independent theoretical methods were employed to search for candidate structures of BC_5 at ambient pressure. In the first method, random structures were generated with the "random search" approach.[5] Two batches of 200 random BC_5 structures were generated with models containing 1 and 2 BC_5 units per primitive cell and then fully optimized using first-principles calculations. The second method involved an exhaustive generation of all possible BC_5 structures by placing four-coordinated (sp^3) C atoms in either a 6-atom or 12-atom cell with cubic diamond framework. Once a unit cell is constructed, each C site in the 6-atom cell or a combination of two C sites in a 12-atom cell is replaced by B atoms and the resulting BC_5 structures are then fully optimized. Structural optimizations were performed with the Vienna *ab initio* simulation package (VASP) code[6] employing projector-augmented wave (PAW) potentials[7] with a generalized gradient approximation Perdew-Burke-Ernzerhof (GGA-PBE).[8] Both search methods produced the same candidates for stable lowest-energy structures. The equations of state (EOS) and enthalpies for candidate structures were calculated with the VASP and two separated PAW potentials with local-density approximation Perdew-Zunger (LDA-PZ) (Ref. 9) and GGA-PBE. Refined Monkhorst-Pack meshes[10] were used for the EOS and enthalpies calculations. A $20\times20\times8$ *k*-point mesh was used for $P3m1$ structure and a $16\times16\times16$ *k*-point mesh was used for $I\bar{4}m2$, $Imm2$, and $P\bar{1}$ structures. Elastic and shear moduli were calculated for candidate structures using the stress-strain relations[11] with the MATERIALS TOOLKIT software[12] together with a least-squares fitting using calculated strains[11] in the range 0.3–0.7 %. Band structure, density of states (DOS), Raman spectra, phonon and electron-phonon coupling calculations were performed using the QUANTUM ESPRESSO code[13] with norm-conserving GGA-PBE pseudopotentials in the Troullier-Martins form.[14] Raman frequencies were calculated using a $10\times10\times4$ *k*-point mesh for $P3m1$ structure and a $8\times8\times8$ *k*-point mesh for $I\bar{4}m2$ and $P\bar{1}$ structures. The phonon band structure for $I\bar{4}m2$ structure was calculated using a $6\times6\times6$ *q*-point mesh with individual phonon matrices calculated from a $12\times12\times12$ *k*-point mesh. The EPC matrices for $I\bar{4}m2$ structure have been calculated on a $6\times6\times6$ *q* point with individual matrices obtained using a $24\times24\times24$ *k*-point mesh.

Analysis of the optimized structures showed that structures with one BC_5 primitive cell are energetically more favorable than those composed of B_2C_{10} primitive cells. Moreover, two classes of structures were revealed. Within the scope of the structural search in the present study, i.e., among the models containing 1 and 2 BC_5 units per primitive cells, the more stable structures often have second-nearest B atoms bridged by a C atom and those without are higher in energy.

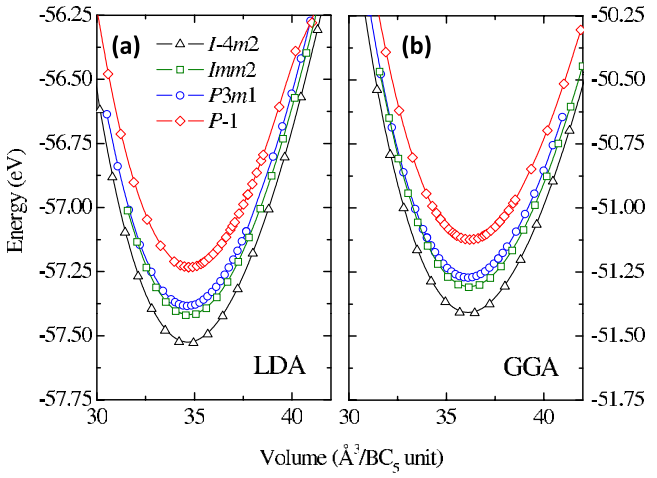

FIG. 1. (Color online). Calculated EOS of four BC_5 candidate structures using (a) LDA-PZ and (b) GGA-PBE potentials.

The calculated EOS using both LDA-PZ [Fig. 1(a)] and GGA-PBE [Fig. 1(b)] show that the three lowest-energy structures have $I\bar{4}m2$, $Imm2$, and $P3m1$ space-group symmetries, and all consist of one BC_5 primitive cell. A $P\bar{1}$ structure with a B_2C_{10} primitive cell [Figs. 1(a) and 1(b)] has higher energy but fits well with the x-ray diffraction pattern reported at 2200 K [Fig. 2(a)]. The order of stability at ambient pressure is $I\bar{4}m2 > Imm2 > P3m1 > P\bar{1}$ and the energy of $I\bar{4}m2$ structure is significantly lower than that of other structures. The structural details of the four candidate structures are listed in the Table I. Since the superhard BC_5 was synthesized at 24 GPa in experiment,[3] it is necessary also to examine the order of stability of the four candidate structures at high pressure. The enthalpies of the four candidate structures at high pressure were therefore calculated up to above 50 GPa and no difference was found in the order of stability

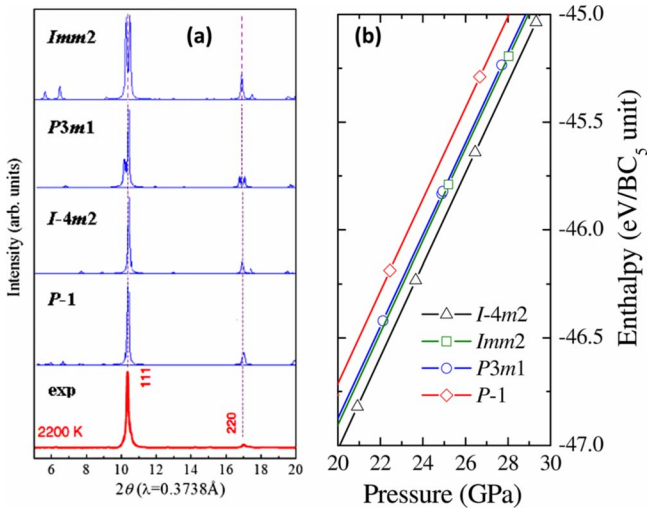

FIG. 2. (Color online). (a) Calculated and experimental x-ray diffraction patterns of BC_5 structures at 24 GPa. Experimental data (Ref. 3) were measured at 2200 K and the calculations were performed at 0 K. (b) Calculated enthalpies of four BC_5 candidate structures between 20 and 30 GPa using the GGA-PBE potential.

from that at ambient pressure. Figure 2(b) shows the calculated enthalpies of the four candidate structures between 20 and 30 GPa using GGA-PBE potential. It is clear that at 24 GPa, the order of stability for the four candidate structures is still $I\bar{4}m2 > Imm2 > P3m1 > P$-1. The same calculation using LDA-PZ potential (not shown) yielded the same enthalpy order at high pressure. Previously, the $P3m1$ structure was predicted to be the most stable structure with 1 and 2 BC_5 units per cell.[15] The emergence of the two more stable $I\bar{4}m2$ and $Imm2$ structures illustrates the power of the two different structural search methods used in the present study. The $I\bar{4}m2$ and $P3m1$ structures have similar structural motifs and both consist of stackings of a "B-layer" sandwiched between every five layers of C. The $Imm2$ structure consists of rows of B atom bridged by C atoms. The $P\bar{1}$ structure does not have any second-nearest-neighbor B atoms.

The predicted energy order and the nature of chemical bonding in these four BC_5 polymorphs can be explained by multicenter bonding between B and C. In a classical (Lewis covalent) bond, two valence electrons are shared with two adjacent centers ($2c$-$2e$). For all the BC_5 polymorphs discussed here, both the B and C atoms have local tetrahedral bonding (sp^3 hybridization). Unlike C atom, a B atom has only three valence electrons and there are not sufficient electrons (electron deficiency) to form four $2c$-$2e$ bonds. Therefore, valence electrons are shared among the B-C-B unit forming two nonclassical three-center two-electron ($3c$-$2e$) bonds. This multicenter description of the B-C-B bond is well established for carboranes[16,17] and has been applied recently to describe the structure of α- and γ-B.[18] The multicenter bonding is equally described by resonance structures,[19]

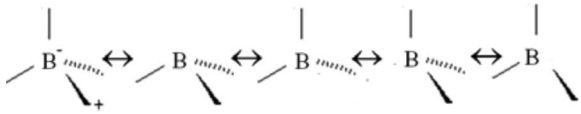

The existence of resonance structures implies a delocalization of electron density. The delocalization of valence electrons in the B-C-B bonds or planes is confirmed in the electronic band-structure calculations. As seen from Fig. 3(a), in the $I\bar{4}m2$ structure, the B atoms are located in the $2d$ symmetry site while the C atoms are located in three different symmetry sites, $2b$, $4f$, and $4e$. The B-C-B bonds are constructed with the B atoms ($2d$) and their nearest-neighboring C atoms at $4e$ symmetry site. The calculated DOS for $I\bar{4}m2$ structure in Fig. 3(b) clearly shows that the electronic states near the Fermi level are derived mainly from these two groups of atoms. The calculated total DOS at the Fermi level for the $I\bar{4}m2$ structure is 1.16 $e^-/eV/BC_5$, for which 80% is from the B atoms ($2d$) and their nearest-neighboring C atoms ($4e$). In other words, the DOS at the Fermi level is dominated by the B-C-B bonds, which gives rise to weak metallic character.[15] The electron deficiency of B atoms creates empty bands above the Fermi level and these bands are dominated by the sp^3-hybridized B-C-B bonds. This fact suggests that the transport properties, such as conductivity, are essentially

TABLE I. Optimized structural parameters for BC_5 candidate structures at ambient pressure.

Space group	Lattice parameters (Å, deg)			Atomic coordinates (Fractional)		
$I\bar{4}m2$	$a=2.525$, $c=11.323$	B	$2d$	0.5000	0.0000	0.2500
		C	$4e$	0.0000	0.0000	0.1568
		C	$2b$	0.0000	0.0000	0.5000
		C	$4f$	0.0000	0.5000	0.0805
$Imm2$	$a=7.731$, $b=2.503$, $c=3.736$	B	$2b$	0.5000	0.0000	0.0233
		C	$4c$	0.1725	0.5000	0.2835
		C	$4c$	0.1686	0.0000	0.0419
		C	$2a$	0.0000	0.0000	0.8260
$P3m1$	$a=2.553$, $c=6.392$	B	$1a$	0.0000	0.0000	0.0065
		C	$1a$	0.0000	0.0000	0.2599
		C	$1b$	0.3333	0.6667	0.3384
		C	$1b$	0.3333	0.6667	0.5820
		C	$1c$	0.6667	0.3333	0.6643
		C	$1c$	0.6667	0.3333	0.8999
$P\bar{1}$	$a=4.455$, $b=4.459$, $c=4.462$ $\alpha=119.89$, $\beta=80.81$, $\gamma=79.80$	B	$2i$	0.8104	0.3946	0.7319
		C	$2i$	0.3149	0.2165	0.8855
		C	$2i$	0.6833	0.0964	0.7719
		C	$2i$	0.2006	0.2693	0.6014
		C	$2i$	0.3171	0.5600	0.5752
		C	$2i$	0.8118	0.0638	0.0632

determined by the B-C-B bonds. As shown in Fig. 3(a), the $I\bar{4}m2$ structure is constructed by alternative B-C-B and C-C-C layers along z axis, and therefore, these alternate layers behave as primarily metallic and covalent layers, respectively. This dominance of B-C-B bonds near Fermi level has also been observed for the $P3m1$ structure.[15] However, the calculated total DOS at Fermi level for the $P3m1$ structure is much lower, only 0.77 $e^-/eV/BC_5$, indicating a lower charge-carrier concentration. Since B atoms are bridged by C atoms forming a 2D planar array in $I\bar{4}m2$ structure, this structure is expected to benefit the most from multicenter bonding and should be the most stable polymorph. This assumption was confirmed by the EOS and enthalpy calculations in Figs. 1(a), 1(b), and 2(b). It is perhaps surprising that the "chainlike" structure of $Imm2$ is slightly more stable than the $P3m1$ structure. This can be traced back to the much shorter C^*-C bond length (C^* and C represent C bonded/nonbonded to a B atom) of 1.506 Å as compared to 1.526 Å (both at 24 GPa) in $P3m1$ structure. A shorter C^*-C bond in the $Imm2$ structure indicates stronger C-C interactions. Thus the energy of the $Imm2$ structure is slightly lower than the $P3m1$ structure. Finally, in the $P\bar{1}$ structure, there is no nearest-neighbor B atoms linked by a C atom. Therefore, stabilization from multicenter bonding is expected to be weaker. It should be noted that the relation between the multicenter bonds and corresponding energetics in the B-C systems has also been observed in low-energy polymorphs of BC_3 although the origin was not explained.[20–22] The superconductivity in the $P3m1$ phase of BC_5 has also been attributed to delocalized electrons along B-C-B bonds.[15]

The calculated diffraction patterns for the four candidate structures at 24 GPa are compared with the observed pattern[3] measured at the same pressure but at high temperature (2200 K) in Fig. 2(a). The $P3m1$ and $Imm2$ structures can therefore probably be eliminated as possible candidates. The calculated $P\bar{1}$ pattern apparently is in better agreement with experiment even though it has lower symmetry. For $I\bar{4}m2$ structure, the pair of Bragg peaks predicted at ~17° is not observed. Additional calculations show that the relative intensity of these peaks is pressure dependent and the splitting of 0.5° is larger than the experimental resolution. The very small deviation of diffraction pattern of the $P\bar{1}$ structure from that of diamond is due to a minor perturbation of the crystal structure by homogenous B doping rather than 2D clustering. The $P\bar{1}$ space group resulting from a particular B position doping is only one of the many enumerations of randomly placed B atoms in the cubic diamond structure. The experimental diffraction pattern could therefore be the average of several possible structures. The local environments at the C atoms in the homogeneously doped structures, even those bonded to B, are not heavily distorted from ideal tetrahedral bonding. The C-C distances in the $P\bar{1}$ structure at 24 GPa is 1.52 Å with a B-C-C angle of 103.6°. The B-C distances are about 1.61–1.62 Å with C-B-C angles atom range from 100.5° to 109.8°. Note that B in synthesized BC_5 is almost certainly disordered[3] and the $P\bar{1}$ structure simply is one of many similar structures. The disordering results in an overall cubic symmetry.

A comparison of the calculated Raman-active vibration frequencies with the experimental spectrum[3] is shown in Fig.

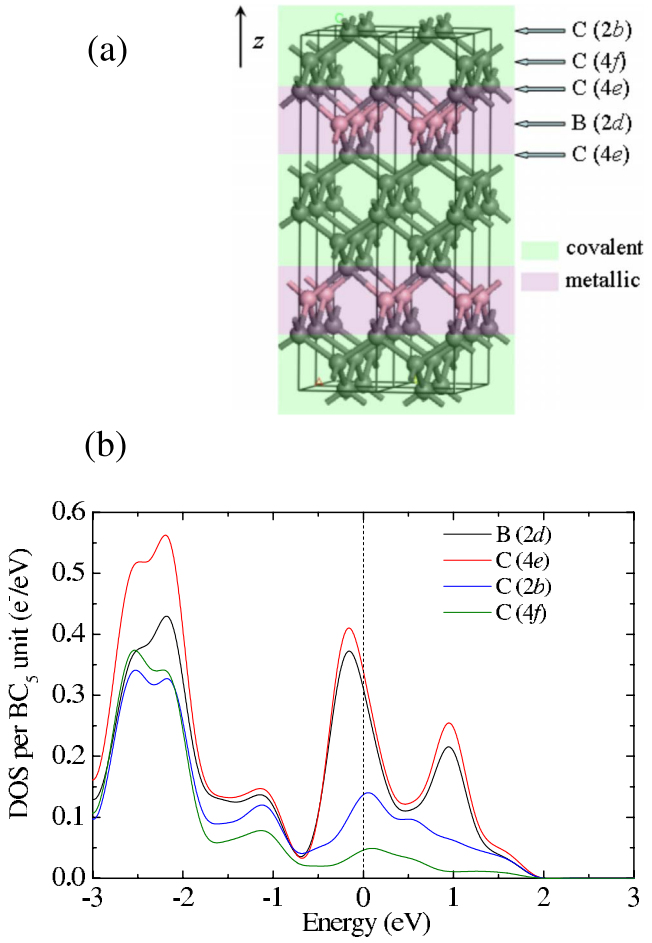

FIG. 3. (Color online). (a) Construction of the $I\bar{4}m2$ structure by alternating B-C-B and C-C-C layers along z axis. The site symmetries for the C atoms ($2b$, $4f$, and $4e$) and B atoms ($2d$) are marked. (b) Calculated DOS of the $I\bar{4}m2$ structure projected to each type of atom and to each symmetry site at ambient pressure.

4. The $P\bar{1}$ structure gives the best overall agreement in both the range of the Raman bands, from 480 to 1300 cm^{-1}, and in the absolute frequencies with the observed prominent features. The highest-energy vibration observed at 1296 cm^{-1} redshifted from pure diamond by 36 cm^{-1} is correctly reproduced by the calculation at 1274 cm^{-1} with a shift of 26 cm^{-1}. The Raman features at 887 and 1002 cm^{-1} are also consistent with the calculated vibrations at similar energies. In contrast, no Raman-active bands are predicted for the $I\bar{4}m2$ structure between 790 and 1050 cm^{-1}. Moreover, the highest-energy Raman vibration was calculated to be at 1205 cm^{-1}, which is almost 100 cm^{-1} redshifted from the calculated diamond frequency.

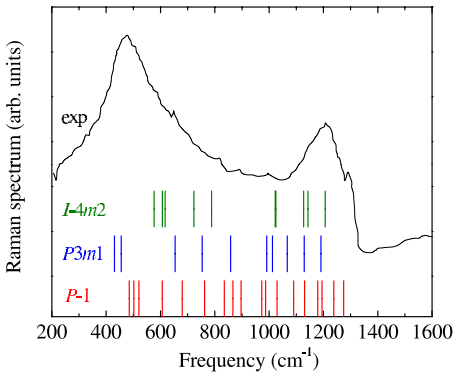

FIG. 4. (Color online). Comparison of calculated vibration frequencies (tick marks) and experimental Raman spectra (Ref. 3) of BC_5 candidate structures at ambient pressure.

The measured Vicker's hardness for BC_5 is 71 GPa.[3] It has been suggested that the hardness of a material can be correlated with its bulk modulus[23] and shear modulus[24] although hardness is clearly recognized to be a complex function of many other of the properties of a crystal. Using the correlation proposed in Ref. 24, for example, and experimental hardness of diamond of 115 GPa and a shear modulus of 545 GPa, the hardness for $I\bar{4}m2$ and $P\bar{1}$ are estimated to be 80 and 79 GPa, respectively. The bulk moduli (B_0) for $I\bar{4}m2$ and $P\bar{1}$ are 376 and 370 GPa, with pressure derivatives (B_0') 3.9 and 3.6 were obtained from fits of the theoretical equations of state to a third-order Murnaghan equation.[25] These values are consistent with the experimental value for B_0 of 355(8) GPa and B_0' of 4.5(6). The full set of elastic moduli for $I\bar{4}m2$, $P3m1$, and $P\bar{1}$ are listed in Table II. In view of the synthesis was achieved at HPHT, it is not unreasonable that a metastable phase with homogenous B doping can be recovered. Moreover, the calculated Voigt and Reuss shear moduli[26] for $I\bar{4}m2$ and $P3m1$ of 379 and 377 GPa, respectively, both are slightly higher than 374 GPa for $P\bar{1}$. Phonon-dispersion calculations show the $P\bar{1}$ structure is dynamically unstable at 0 K. The Born stability conditions,[27] which are used to verify mechanical stability, were evaluated by calculating the determinants of the principal minors of the quadratic form of the matrix for the C_{ij} shown in Table II. The determinants are all positive indicating mechanical stability and therefore the $P\bar{1}$ structure may be entropically stabilized at high temperatures. At ambient pressure, the calculated total energy of $P\bar{1}$ is about 0.3 eV/BC_5 unit (0.05 eV/atom) higher than that of $I\bar{4}m2$ [Figs. 1(a) and 1(b)]. This energy difference is slightly larger than that between graphite and diamond (0.024 eV/atom).[28] The theoretical results provide support that recovered BC_5 has a B-disordered cubic structural motif similar to that of the $P\bar{1}$ structure. The experimental conditions[3] employed in the synthesis of cubic BC_5 therefore apparently favor a homogenous distribution of B over clustering such as would be found in a $I\bar{4}m2$ structure.

The most significant result in the present study is the prediction of the lowest-energy superhard $I\bar{4}m2$ structure within the basic BC_5 diamondlike framework. This structure is found to be elastically and dynamically stable from phonon calculations [Fig. 5(a)]. The band structures of $I\bar{4}m2$ and cubic diamond are presented in Fig. 5(b), both calculated at ambient pressure. In $I\bar{4}m2$ structure, the Fermi level is shifted down by 1.7 eV with respect to the top of valence bands. Compared with diamond, a substantial change is seen at point M in $I\bar{4}m2$ band structure. The degeneracy at M point is removed and as a result, several steep (dispersive)

TABLE II. Components of the calculated elastic constants (in GPa) for $I\bar{4}m2$, $P3m1$, and $P\bar{1}$ phases of BC_5. The top table defines the notation for the tables containing the elastic moduli.

C_{ij}	C_{11}	C_{12}	C_{13}	C_{14}	C_{15}	C_{16}
	C_{21}	C_{22}	C_{23}	C_{24}	C_{25}	C_{26}
	C_{31}	C_{32}	C_{33}	C_{34}	C_{35}	C_{36}
	C_{41}	C_{42}	C_{43}	C_{44}	C_{45}	C_{46}
	C_{51}	C_{52}	C_{53}	C_{54}	C_{55}	C_{56}
	C_{61}	C_{62}	C_{63}	C_{64}	C_{65}	C_{66}
$I\bar{4}m2$	775 GPa	175	169	0	0	0
	175	775	169	0	0	0
	169	169	830	0	0	0
	0	0	0	479	0	0
	0	0	0	0	479	
	0	0	0	0	0	304
$P3m1$	862 GPa	166	88	−110	0	0
	166	862	88	110	0	0
	88	88	992	0	0	0
	−110	110	0	397	0	0
	0	0	0	0	397	−110
	0	0	0	0	−110	348
P-1	1004 GPa	51	67	9	−13	31
	51	987	128	1	−78	−12
	67	128	964	−16	84	−10
	9	1	−16	84	24	−85
	−13	−78	84	24	287	−21
	31	−12	−10	−85	−21	273

bands cross the Fermi surface along $\Gamma \rightarrow M \rightarrow X$. These steep bands are responsible for the electron conduction and primarily sustained in the B-C-B bonds [Fig. 3(a)]. On the other hand, a flat (non-dispersive) band located approximately 0.4 eV above the Fermi level is found near M in the $M \rightarrow X$ direction [Fig. 5(b)]. The simultaneous occurrence of steep and flat bands close to the Fermi level has been suggested as characteristics favoring a superconducting state.[29–32] It was proposed that the chemical origin of conventional superconductivity was associated with the pairing of localized electrons close to the Fermi surface.[29] In an equivalent presentation, it was suggested that the Fermi-surface nesting becomes larger if the velocities of the electrons are small and/or collinear.[33] Provided this hypothesis is correct, the flat bands close to the Fermi level, as the velocities of electrons are vanishing, sets up a favorable condition for electron pairing.[34,35] The delocalized electrons in the steep bands interact with the flat bands through lattice vibrations (phonons) and provide significant contribution to the EPC. The phonons modulate the bonding character in the system and cause a dynamic vibration of the Fermi level. The steep bands serve as a reservoir for delocalized electrons. Once an empty flat band is brought below the Fermi level, the delocalized electrons will scatter into the flat band, become localized and tend to form Cooper pairs. Once a filled flat band vibrates above the Fermi level, the Cooper pairs will scatter back into the steep band. As the flat band close to the Fermi level is periodically depleted and filled due to the lattice vibration, more and more Cooper pairs are created.[29] For $I\bar{4}m2$ structure, the delocalized electrons sustained in the B-C-B bonds are coupled with the high-frequency B-C vibrations [Fig. 5(a)], which set favorable condition for a large EPC parameter λ and average vibrational frequency ($\omega_{\log}$).[34] To investigate the possibility of superconductivity in $I\bar{4}m2$ structure, EPC calculations were performed.[13] At ambient pressure, the calculated λ and $\omega_{\log}$ for $I\bar{4}m2$ structure are 0.89 and 810 K. Applying the Allen-Dynes extension of the McMillan equation[36] and using a nominal values of the Coulomb repulsive parameter (μ^*) of 0.1, a superconductivity critical temperature (T_c) of 47 K is estimated. The predicted T_c is almost identical to that previously reported for the $P3m1$ phase of BC_5. The $P3m1$ structure was predicted to be a superconductor[15] with an estimated T_c of 45 K. Diluted doped diamond has shown to be a superconductor.[37,38] Analysis of distribution of phonon linewidth in the first Brillouin zone shows that the electronic states near the M point contribute almost 22% to the total λ. Considering the M point is where the steep bands and flat bands cross, this result seems to support the steep band—flat-band scenario for the occurrence of superconductivity. This result is encouraging

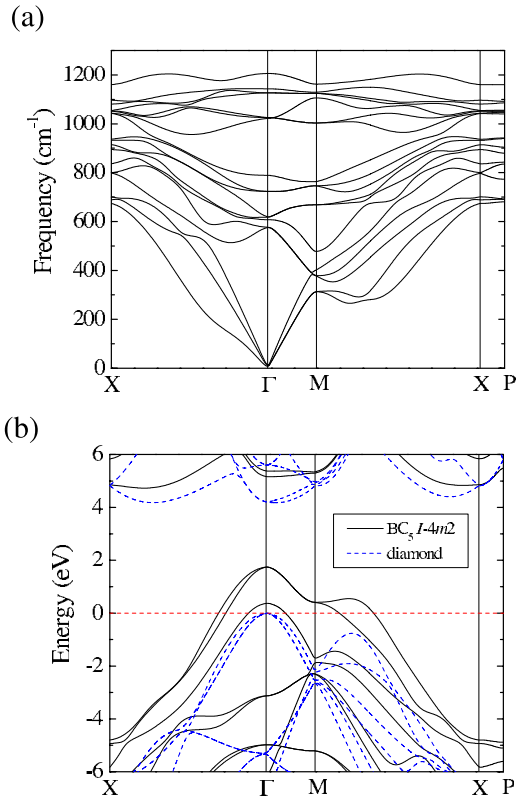

FIG. 5. (Color online). (a) Calculated phonon band structure of the $I\bar{4}m2$ structure at ambient pressure. (b) Calculated electron band structure of the $I\bar{4}m2$ structure compared with that of diamond within the $I\bar{4}m2$ unit cell at ambient pressure.

since $I\bar{4}m2$ is the thermodynamically most stable structure for BC_5 and may be possible to synthesize employing HPHT methods with carefully chosen experimental conditions to control the kinetics such as lower temperature or longer annealing time. At ambient temperature, $I\bar{4}m2$ is a metal and is predicted to be harder than the experimental value[3] for cubic BC_5. It becomes a superconductor at low temperature.

In summary, it is shown here the recently synthesized diamondlike BC_5 (Ref. 3) is a metastable phase. A thermodynamic stable polymorph of BC_5 was revealed from structural searches. This phase is superhard and superconducting with an estimated superconducting critical temperature of 47 K. A unique structural feature is the presence of B-C-B chains forming 2D layers sandwiched between tetrahedrally bonded diamondlike C layers. Similar B-C-B chains have also been found previously in a superhard form of BC_3 (Ref. 22). Multicenter bonding along the B-C-B chains results in the delocalization of valence electrons and is responsible for the metallic character. The stability of hard BC_x polymorphs can be attributed to this common structural motif. Multicenter bonding in electron-deficient carboranes is well known in chemistry.[16–19] The chemical bonding can be described alternatively by the valence-bond theory invoking the existence of resonance structures. This description of bonding is relevant to a recent suggestion on the mechanism in boron-doped diamond by the resonating valence-bond model.[39–41] In diamond, the C atoms are bonded to their neighbors through sp^3 hybridization. The substitution of a C atom by a B impurity, which has one less electron, leaves a hole (an unpaired spin) behind in an otherwise filled band. In the ground state this hole is bound to the B atom. The coupling between singlet spins of neighboring neutral B atoms resonate with B^+ and B^- free carriers states resulting in a resonating valence-bond superconducting state.[41]

*Author to whom correspondence should be addressed; john.tse@usask.ca

[1] *The Nature of Diamonds*, edited by G. E. Harlow (Cambridge University Press, New York, 1998).
[2] V. L. Solozhenko, N. A. Dubrovinskaia, and L. S. Dubrovinsky, Appl. Phys. Lett. **85**, 1508 (2004).
[3] V. L. Solozhenko, O. O. Kurakevych, D. Andrault, Y. Le Godec, and M. Mezouar, Phys. Rev. Lett. **102**, 015506 (2009).
[4] M. M. Balakrishnarajan, P. D. Pancharatna, and R. Hoffmann, New J. Chem. **31**, 473 (2007).
[5] C. J. Pickard and R. J. Needs, Phys. Rev. Lett. **97**, 045504 (2006).
[6] G. Kresse and J. Furthmüller, Comput. Mater. Sci. **6**, 15 (1996).
[7] G. Kresse and D. Joubert, Phys. Rev. B **59**, 1758 (1999).
[8] J. P. Perdew, K. Burke, and M. Ernzerhof, Phys. Rev. Lett. **77**, 3865 (1996).
[9] J. P. Perdew and A. Zunger, Phys. Rev. B **23**, 5048 (1981).
[10] H. J. Monkhorst and J. D. Pack, Phys. Rev. B **13**, 5188 (1976).
[11] Y. Le Page and P. Saxe, Phys. Rev. B **65**, 104104 (2002).
[12] Y. Le Page and J. R. Rodgers, J. Appl. Crystallogr. **38**, 697 (2005).
[13] QUANTUM-ESPRESSO is a community project for high-quality quantum simulation software, based on density-functional theory, and coordinated by Paolo Giannozzi. See http://www.quantum-espresso.org and http://www.pwscf.org
[14] N. Troullier and J. L. Martins, Phys. Rev. B **43**, 1993 (1991).
[15] M. Calandra and F. Mauri, Phys. Rev. Lett. **101**, 016401 (2008).
[16] D. S. Marynick and W. N. Lipscomb, J. Am. Chem. Soc. **94**, 1748 (1972).
[17] W. N. Lipscomb, Acc. Chem. Res. **6**, 257 (1973); Science **196**, 1047 (1977).
[18] P. Rulis, L. Wang, and W. Y. Ching, Phys. Status Solidi (RRL) **3**, 133 (2009).
[19] *Nature of Chemical Bond and the Structure of Molecules and Crystal: An Introduction to Modern Structural Chemistry*, edited by L. Pauling (Cornell University Press, Ithaca, New York, 1960).
[20] J. Yang, H. Sun, J. He, Y. Tian, and C. Chen, J. Phys.: Condens. Matter **19**, 346223 (2007).
[21] J. E. Lowther, J. Phys.: Condens. Matter **17**, 3221 (2005).
[22] Z. Liu, J. He, J. Yang, X. Guo, H. Sun, H. T. Wang, E. Wu, and Y. Tian, Phys. Rev. B **73**, 172101 (2006).
[23] M. L. Cohen, Annu. Rev. Mater. Sci. **30**, 1 (2000).
[24] M. Teter, MRS Bull. **23**, 22 (1998).
[25] F. Birch, Phys. Rev. **71**, 809 (1947).
[26] G. Grimvall, *Thermophysical Properties of Materials* (Elsevier, New York, 1999).
[27] M. Born and K. Huang, *Dynamical Theory of Crystal Lattices* (Oxford University Press, New York, 1954).
[28] M. T. Yin and M. L. Cohen, Phys. Rev. Lett. **50**, 2006 (1983).
[29] A. Simon, Angew. Chem., Int. Ed. Engl. **36**, 1788 (1997).
[30] S. Deng, A. Simon, and J. Köhler, Angew. Chem., Int. Ed. Engl. **37**, 640 (1998).
[31] S. Deng, A. Simon and J. Köhler, J. Supercond. **16**, 477 (2003).
[32] S. Deng, A. Simon, and J. Köhler, J. Am. Chem. Soc. **124**, 10712 (2002).
[33] D. Kasinathan, J. Kuneš, A. Lazicki, H. Rosner, C. S. Yoo, R. T. Scalettar, and W. E. Pickett, Phys. Rev. Lett. **96**, 047004 (2006).
[34] J. S. Tse, Y. Yao, and K. Tanaka, Phys. Rev. Lett. **98**, 117004 (2007).
[35] Y. Yao and J. S. Tse, Phys. Rev. B **75**, 134104 (2007).
[36] P. B. Allen and R. C. Dynes, Phys. Rev. B **12**, 905 (1975).
[37] E. A. Ekimov, V. A. Sidorov, E. D. Bauer, N. N. Mel'nik, N. J. Curro, J. D. Thompson, and S. M. Stishov, Nature (London) **428**, 542 (2004).
[38] Y. Ma, J. S. Tse, T. Cui, D. D. Klug, L. Zhang, Y. Xie, Y. Niu, and G. Zou, Phys. Rev. B **72**, 014306 (2005).
[39] L. Pauling, Phys. Rev. Lett. **59**, 225 (1987).
[40] J. C. Phillips, J. Phys.: Conf. Ser. **108**, 012033 (2008).
[41] G. Baskaran, J. Supercond. Novel Magn. **21**, 45 (2008).